AIP Journal of Applied Physics

High spatial uniformity of photoluminescence spectra in semipolar (20 2 ¯ 1) plane InGaN/GaN quantum wells

K. Gelžinytė, R. Ivanov, S. Marcinkevičius, Y. Zhao, D. L. Becerra, S. Nakamura, S. P. DenBaars, and J. S. Speck

Citation: Journal of Applied Physics **117**, 023111 (2015); doi: 10.1063/1.4905854
View online: http://dx.doi.org/10.1063/1.4905854
View Table of Contents: http://scitation.aip.org/content/aip/journal/jap/117/2?ver=pdfcov
Published by the AIP Publishing

High spatial uniformity of photoluminescence spectra in semipolar $(20\bar{2}1)$ plane InGaN/GaN quantum wells

K. Gelžinytė,[1,2] R. Ivanov,[1] S. Marcinkevičius,[1] Y. Zhao,[3] D. L. Becerra,[3] S. Nakamura,[3] S. P. DenBaars,[3] and J. S. Speck[3]
[1]*Department of Materials and Nano Physics, KTH Royal Institute of Technology, Electrum 229, 16440 Kista, Sweden*
[2]*Institute of Applied Research, Vilnius University, Saulėtekio 9-3, 10222 Vilnius, Lithuania*
[3]*Materials Department, University of California, Santa Barbara, California 93106, USA*

(Received 28 July 2014; accepted 30 November 2014; published online 12 January 2015)

Scanning near-field optical spectroscopy was applied to study spatial variations of emission spectra at room temperature in semipolar $(20\bar{2}1)$ $In_xGa_{1-x}N/GaN$ single quantum wells (QWs) for $0.11 \leq x \leq 0.36$. Photoluminescence (PL) was found to be highly uniform, with peak wavelength deviations and peak intensity deviations divided by average values in the range of 6–12 meV and 0.03–0.07, respectively. Near-field maps of PL parameters showed large, ~5 to 10 μm size areas of similar values, as opposed to 100 nm scale variations, often reported for InGaN QWs. The near-field PL spectra were found to broaden with increasing InN molar fraction. In the low In content QWs, the broadening is primarily determined by the random cation distribution, while for larger InN molar fractions 10 nm scale localization sites with increasingly deeper band potentials are suggested as the linewidth broadening cause. © *2015 AIP Publishing LLC*.
[http://dx.doi.org/10.1063/1.4905854]

I. INTRODUCTION

The semipolar $(20\bar{2}1)$ plane $In_xGa_{1-x}N/GaN$ quantum wells (QWs) have recently been used in high performance light emitting diodes (LEDs) and lasers operating in a wide spectral range from violet to yellow-green.[1–3] Compared to nonpolar *a* or *m* planes of the hexagonal GaN lattice, the semipolar $(20\bar{2}1)$ plane shows higher In incorporation under the same growth conditions,[4] which leads to longer emission wavelengths. Compared to polar *c*-plane QWs, the semipolar ones experience smaller intrinsic electric fields, caused by the difference in spontaneous and piezoelectric polarizations in the well and the barrier layers,[1] which increases the optical transition matrix element and reduces the radiative recombination time.

One of the critical material properties of ternary nitride QWs is the spatial band gap variation. Such variation, which may be caused by composition, QW thickness, and strain inhomogeneities, may affect device performance in different ways. For instance, areas with a lower band gap may contribute to formation of hot spots and premature device degradation.[5] Band inhomogeneities broaden the emission spectra, which may affect gain in laser diodes, since the material gain presumably is inversely proportional to the luminescence linewidth. Besides, spatial band gap variations may correlate with variations of the nonradiative recombination. In some cases, carrier localization at band potential minima reduces the nonradiative recombination rate by isolating carriers from dislocations and related point defect agglomerations, as observed in polar InGaN QWs.[6–8] In other cases, lower potential sites were found to occur in the same regions as an enhanced nonradiative recombination. This effect was observed in green emitting polar InGaN QWs,[7,9] certain semipolar InGaN QWs,[10,11] and AlGaN layers[12] and QWs.[13]

In this work, we probe spatial band gap inhomogeneities in semipolar $(20\bar{2}1)$ QWs by measuring near-field (NF) photoluminescence (PL) spectra. Scanning NF optical microscopy allows mapping optical properties with subwavelength resolution, which has proved to be a powerful tool to study spatial variations of light emission in ternary nitride structures and devices.[6–8,10–15] Particularly, for $(20\bar{2}1)$ InGaN QWs, NF PL measurements were previously reported for just one QW sample with $x \sim 0.30$.[11] Rather large PL intensity variations occurring on a 100 nm scale were observed and assigned to features of the surface morphology. In this work, we explore $(20\bar{2}1)$ single QWs in a wide alloy composition range, $0.11 \leq x \leq 0.36$. The studied QWs show a high spatial uniformity of the emission spectra, which demonstrates a large potential of $(20\bar{2}1)$ QWs for fabrication of efficient and robust light emitting devices operating in a wide spectral range.

II. EXPERIMENT

The studied structures were grown by conventional metal organic chemical vapor deposition (MOCVD) on freestanding low defect density ($\sim 10^6$ cm^{-2}) bulk $(20\bar{2}1)$ plane GaN substrates, provided by Mitsubishi Chemical Corporation. The substrates were treated by chemo-mechanical polishing to produce atomically flat surfaces with the root mean square (RMS) roughness of less than 1 nm. The growth was performed at atmospheric pressure with V/III ratios in excess of 3000 and in N_2 carrier gas. The structures consisted of a 1 μm undoped GaN template layer, a 3 nm thick $In_xGa_{1-x}N$ single QW, and a 10 nm GaN cap layer. The GaN layers were grown with trimethylgallium (TMGa) and ammonia (NH_3) precursors at a growth rate ~10 Å/s and susceptor temperatures ranging between 980 and 1120 °C. The InGaN QW layers

TABLE I. Statistical parameters of the near-field PL scans for the studied QWs.

InN molar fraction	0.11	0.25	0.31	0.34	0.35	0.36
Peak wavelength, average, nm (eV)	418.8 (2.961)	472.4 (2.625)	503.9 (2.461)	535.5 (2.316)	544.7 (2.276)	547.4 (2.265)
Peak wavelength, deviation, nm (meV)	1.07 (7.6)	1.10 (6.1)	1.45 (7.1)	2.57 (11.1)	2.22 (9.2)	2.37 (9.8)
Peak intensity deviation/average	0.031	0.040	0.062	0.063	0.062	0.066
Average FWHM, nm (meV)	14.1 (100)	25.1 (139)	32.4 (160)	39.7 (172)	39.9 (169)	39.6 (165)
FWHM deviation, nm (meV)	0.9 (7.0)	0.9 (5.2)	0.9 (4.4)	1.2 (5.2)	1.8 (7.5)	2.0 (8.3)
Localization parameter σ_L, meV	27.3	42.5	46.8	54.3	54.7	57.8

were grown using triethylgallium (TEGa), trimethylindium (TMIn), and NH_3 precursors at a growth rate $\sim$1 Å/s and susceptor temperatures in the range of 750–900 °C. Indium molar fraction in the QWs of the studied structures was estimated as 0.11, 0.25, 0.31, 0.34, 0.35, and 0.36 (Table I). To estimate the indium content, PL measurements and QW band structure calculations were used. Selected samples were chosen for X-ray diffraction analysis, and the results were consistent with the PL and calculation results. The small thickness of the cap layer was chosen to maintain a good near-field coupling between the NF probe and the QW. It is noteworthy that previous measurements on a $(20\bar{2}\bar{1})$ QW embedded in a LED *p-i-n* structure with a 50 nm thick *p*-side layer produced similar data to the structure with the 10 nm cap layer showing that a longer thermal exposure of the QW during growth of a thicker cap layer does not affect the band potential uniformity of the QW. This makes the present results representative for $(20\bar{2}1)$ light emitting devices as well.

Near-field PL scans were performed at room temperature with a scanning NF optical microscope (SNOM) operating in the illumination-collection mode. Aluminum-coated UV fiber probes with 50 to 150 nm aperture diameters were used. PL was excited directly into the QWs by 200 fs pulses from a frequency doubled Ti:sapphire laser with a 390 nm central wavelength. The photoexcited carrier density, evaluated from the average excitation power density, the probe throughput, the aperture diameter, and the InGaN absorption coefficient was below $2 \times 10^{11}\,\mathrm{cm}^{-2}$. For PL detection, a spectrometer equipped with a liquid nitrogen cooled CCD detector was used. Typical areas of $20 \times 20\,\mu\mathrm{m}^2$ were scanned with a 200 nm step. In search of fine, 100 nm scale details, scans were also performed on smaller areas from $1 \times 1\,\mu\mathrm{m}^2$ to $6 \times 6\,\mu\mathrm{m}^2$ with steps from 33 nm to 100 nm. In the large area scans, the spatial resolution was limited by the step size and in the small area scans — by the probe aperture diameter. An entire QW PL spectrum was recorded at each point of a scan. Due to the multimode character of the optical fiber, PL polarization was not resolved.

III. EXPERIMENTAL RESULTS

The large variation of the InGaN composition resulted in a wide span of the emission spectra with peak wavelengths ranging from 419 to 548 nm. Fig. 1(a) displays selected NF spectra. With increased In content, the spectra shift to longer wavelengths and broaden. In most cases, the spectra have a Gaussian shape with no fine structure, such as multiple peaks or shoulders. Only for the largest InN molar fractions, some structure in the peaks appears. Far-field PL spectra (Fig. 1(b)) have similar shapes and are just slightly wider than the NF spectra. This hints at the high spatial homogeneity of the QWs. Far-field PL parameters are similar to the average NF data presented in Table I.

Figure 2 shows surface morphology images measured by atomic force microscopy (AFM) for the four samples from Fig. 1. One can notice shallow ridge structures aligned along the $[\bar{1}2\bar{1}0]$ direction. These features are similar to the ones observed in $(20\bar{2}1)$ InGaN/GaN QWs previously.[11] The studied structures are smooth with RMS values between 0.7 and 1.3 nm, i.e., similar to those of the GaN substrate. The key observation for the future discussion is that there is no pronounced correlation between the AFM and the SNOM maps.

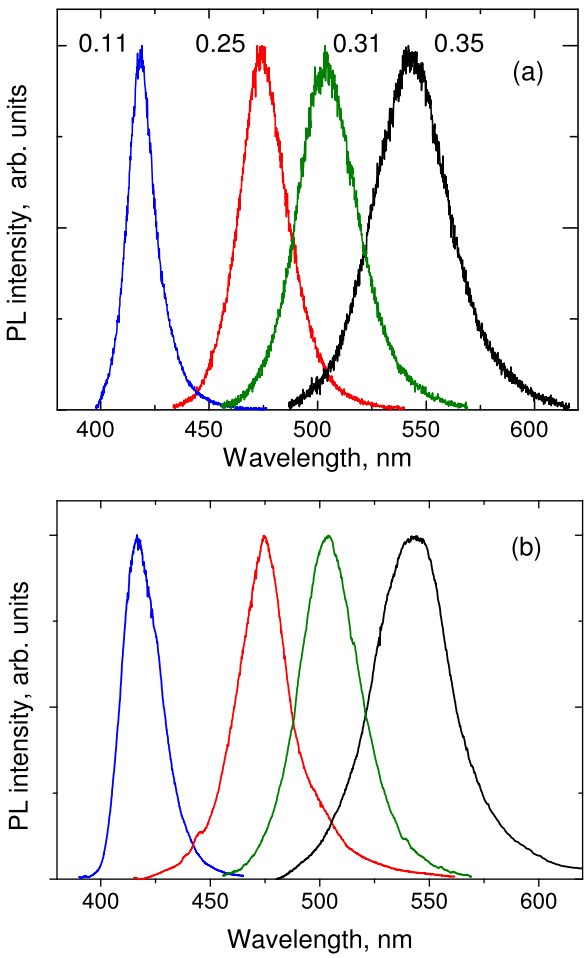

FIG. 1. Selected normalized near-field (a) and far-field (b) PL spectra for $(20\bar{2}1)$ $In_xGa_{1-x}N$ QWs with 0.11, 0.25, 0.31, and 0.35 InN molar fractions.

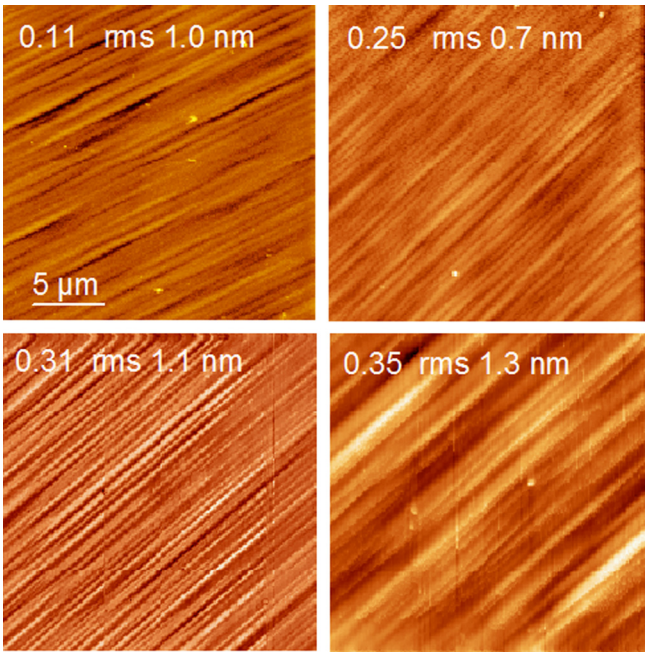

FIG. 2. $20 \times 20\,\mu$m AFM scans of surface morphology for $(20\bar{2}1)$ $In_xGa_{1-x}N$ QWs with 0.11, 0.25, 0.31, and 0.35 InN molar fractions.

Let us look into the details of the NF PL scans of the different QWs. The $In_{0.11}Ga_{0.89}N$ QW shows spatially very uniform spectra. Maps of the peak wavelength, the peak intensity, and the full width at half maximum (FWHM) are shown in Fig. 3. As can be judged from the figure, the peak wavelength and the FWHM have very small variations. Quantitatively, this is reflected in small peak wavelength and FWHM standard deviations, 1.1 nm and 0.9 nm, respectively (Table I). Small area high spatial resolution scans have not revealed any 100 nm scale features, often observed in InGaN QWs.[7,11,14,15] This shows that In incorporation during the growth of low In content QWs is very uniform.

The PL peak intensity (Fig. 3(b)) and the spectrally integrated intensity (not shown) maps display larger variations, even though the ratio of the deviation and the average value is only 0.03. In the intensity map, apart from large areas with similar intensity values, one can observe a few lower intensity regions. These areas do not have corresponding features in the peak wavelength map; thus, they are not related to lower potential sites with a faster nonradiative recombination, sometimes observed in ternary nitrides.[7,12] Rather, the enhanced nonradiative recombination takes place in areas with a wide, extended state band gap. Most probably, the lower intensity areas have a larger density of extended and point defects. For a likely dislocation density of $5 \times 10^6\,cm^{-2}$, a scanned area of $20 \times 20\,\mu m^2$ should contain ~40 dislocations. In Fig. 3(b), one can spot 8–10 regions with a lower PL intensity. Some of them extend for a few μm, thus, they might contain dislocation clusters rather than individual defects.[16] However, such lower intensity spots do not appear in all scans. Thus, dislocations alone cannot account for areas with an increased rate of the nonradiative recombination. Probably, it is the threading dislocation — point defect agglomerations that act as the nonradiative recombination centers.[17] Other extended defects, such as stacking faults, should not be

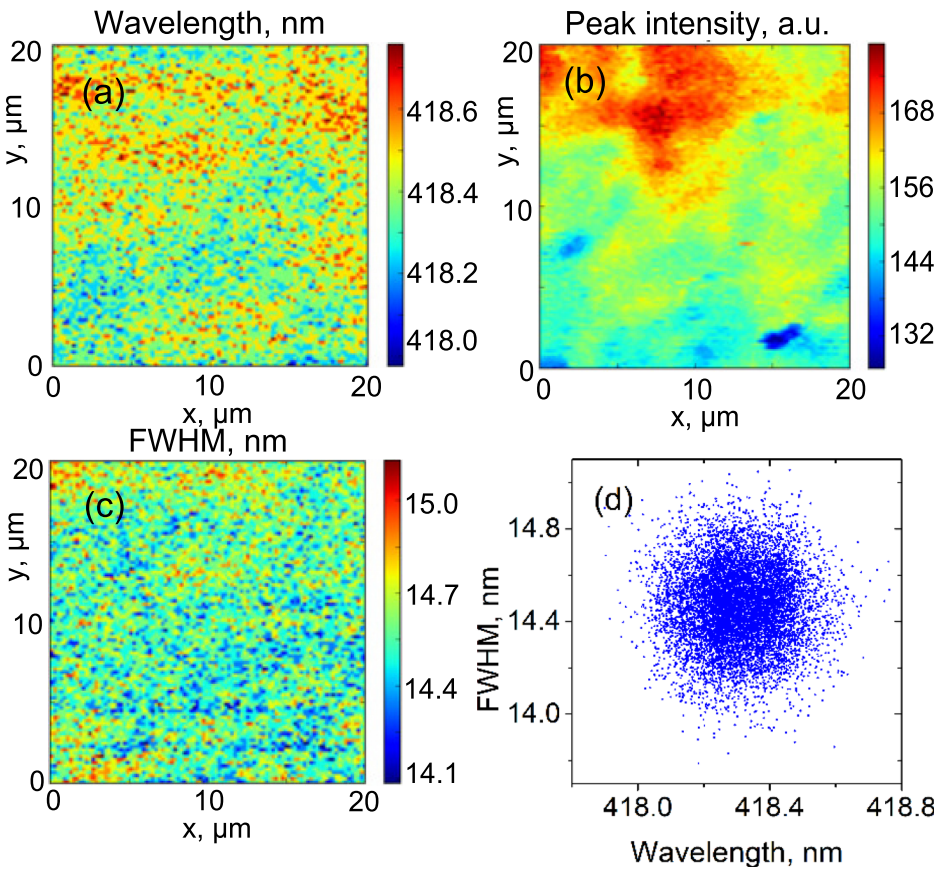

FIG. 3. NF PL maps of the peak wavelength (a), the peak intensity (b) and the FWHM (c), and correlation between the FWHM and the peak wavelength (d) for the $In_{0.11}Ga_{0.89}N$ QW.

important for these narrow $(20\bar{2}1)$ QWs.[18] One should note, however, that the PL intensity reduction in the low intensity spots is only 10%–20%; thus, such features should not be critical for device performance.

Correlations between the peak wavelength and the FWHM (Fig. 3(d)), and the peak intensity and the FWHM, are negligible; for both the Pearson product-moment correlation coefficient r is equal to 0.03. No correlation between the PL intensity and the peak wavelength indicates that recombination rates at the higher and lower potential sites are the same. This is in accordance with the small peak wavelength variations and points at the absence of deep localization centers with properties different from those of the extended states.

The correlation between the peak wavelength and the FWHM increases for the $In_{0.25}Ga_{0.75}N$ QW. Figures 4(a) and 4(b) show the peak wavelength and the FWHM maps. One can clearly notice 3 to 10 μm size areas of longer peak wavelengths and larger FWHM values appearing in the same areas of the scan, which results in a strong correlation with $r = 0.75$ (Fig. 3(c)). Other scans for this sample had smaller, but still positive correlation between the peak wavelength and the FWHM. PL spectra with longer peak wavelengths and broader linewidths correspond to sites with a larger contribution from the lower potential states. However, the data points in the correlation graph (Fig. 4(c)) concentrate towards shorter wavelengths; besides, differences in PL spectra having shorter and longer peak wavelengths are small (Fig. 4(d)). This shows that extended states play the dominating role. The standard peak wavelength and FWHM deviations are essentially the same as for the $x = 0.11$ sample, 1.1 nm and 0.9 nm, respectively. Neither the peak wavelength nor the FWHM correlate with the PL intensity, which shows that in all the scanned area, the recombination properties are similar.

For the $In_{0.31}Ga_{0.69}N$ QW, the peak wavelength and the FWHM maps (Figs. 5(a) and 5(b)) also have large areas of similar values. The apparent pattern of the maps probably does not carry any particular physical meaning (or, at least, it is currently not clear), since other scans of the same sample showed more random islands, similar to the other high In content samples. The correlation between the peak wavelength and the FWHM (Fig. 5(c)) is further increased to $r = 0.82$. The standard peak wavelength and FWHM deviations are small, 1.45 nm and 0.94 nm, respectively, which shows that localization potentials are shallow. The spectra in lower and higher band gap regions hardly differ from each other (Fig. 5(d)). No 100 nm scale variations have been found in the high-resolution scans. This is very different from the previous measurements on $(20\bar{2}1)$ QW with a similar alloy composition.[11] In those measurements, small scale peak wavelength and integrated intensity variations had amplitudes of about 4 to 5 nm and 4 to 8 times, respectively, which correlated with the surface topography and was attributed to the different In uptake for different planes of surface undulations. Our results show that with an optimized MOCVD growth, the nanoscale variations of the emission spectra can be eliminated, and the overall uniformity of the emission spectra drastically improved.

Contrary to the QWs with a lower In indium content, a significant correlation between the peak intensity and the peak wavelength with $r = 0.48$ is found for the

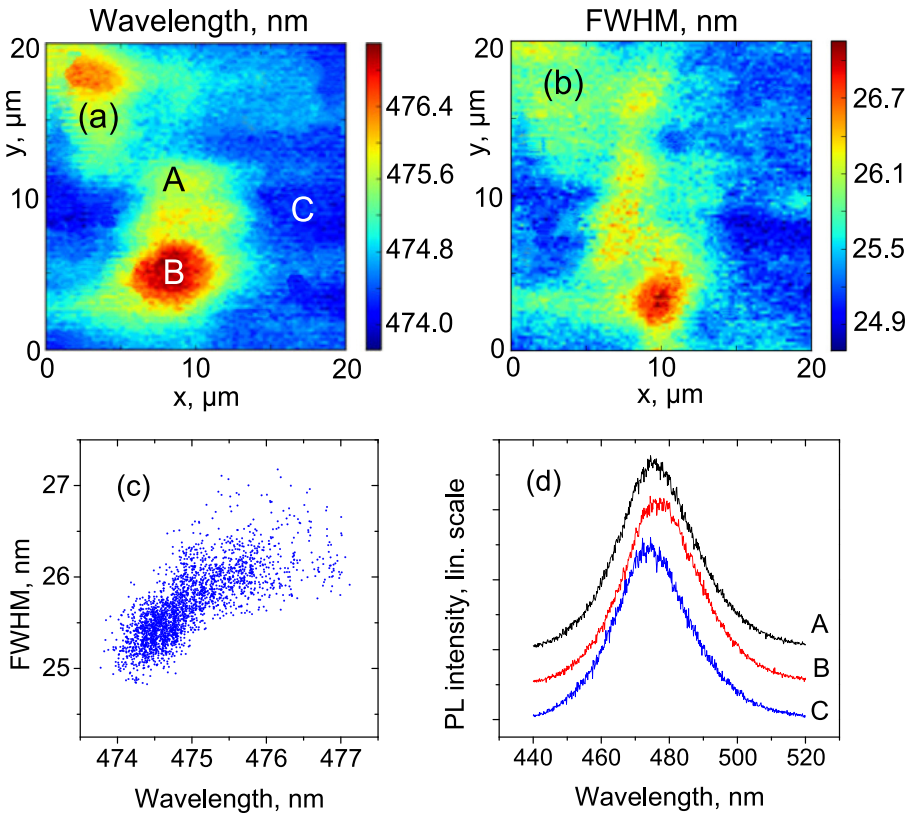

FIG. 4. NF PL maps of the peak wavelength (a) and the FWHM (b), and correlation between them (c) for the $In_{0.25}Ga_{0.75}N$ QW. Part (d) shows spectra, measured at points A, B, and C indicated on the map (a).

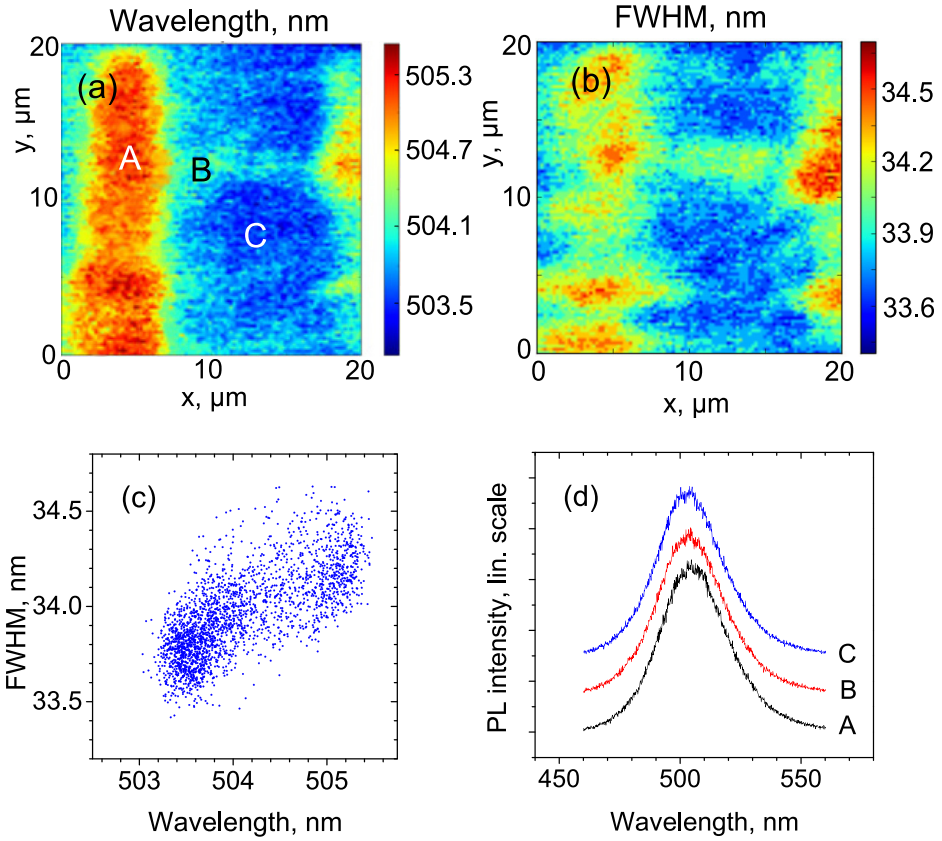

FIG. 5. NF PL maps of the peak wavelength (a) and the FWHM (b), and correlation between them (c) for the $In_{0.31}Ga_{0.69}N$ QW. Part (d) shows spectra, measured at points A, B, and C indicated on the map (a).

$In_{0.31}Ga_{0.69}N$ QW. Such dependence indicates that the lower potential states are deep enough to localize carriers and reduce their diffusion towards the nonradiative recombination centers.

For even higher In content QWs, from 0.34 to 0.36, the peak wavelength and the FWHM variations slightly increase. The peak intensity is still relatively uniform and, in that respect, comparable to the lower In content samples. Fig. 6

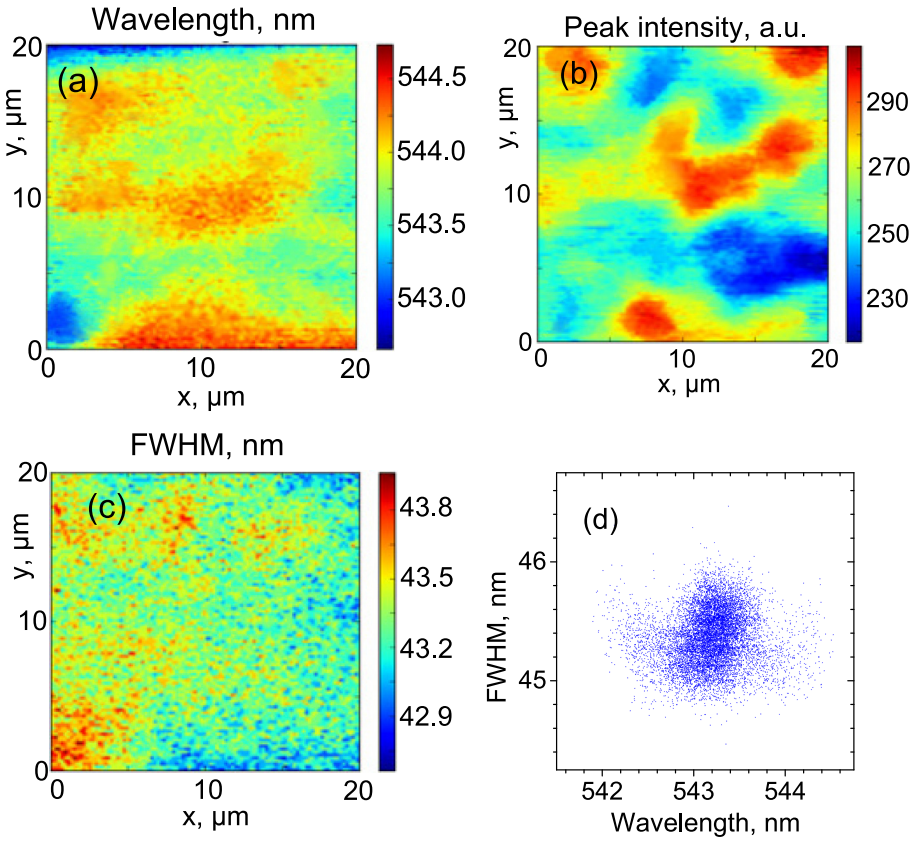

FIG. 6. NF PL maps of the peak wavelength (a), the peak intensity (b) and the FWHM (c), and correlation between the peak wavelength and the FWHM (d) for the $In_{0.35}Ga_{0.65}N$ QW.

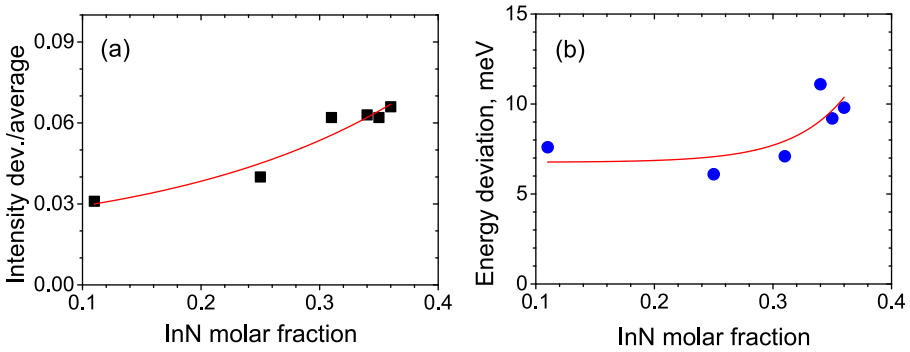

FIG. 7. InGaN composition dependence of the PL peak intensity deviations divided by the average values (a), and the peak wavelength deviations (b).

shows NF PL maps for the $In_{0.35}Ga_{0.65}N$ QW. The peak wavelength deviation for the group of the long wavelength samples is between 2.5 nm and 3 nm (Table I), and the FWHM deviations are from 1.2 nm to 1.8 nm. The correlation between the peak wavelength and the FWHM becomes weaker (Fig. 6(d)) with r values of 0.32 and −0.11 for the 34% and 35% In QWs, respectively. For the $In_{0.36}Ga_{0.64}N$ QW, the correlation further increases in an absolute value to $r = -0.63$.

IV. DISCUSSION

The high spatial uniformity of the optical spectra for all studied QWs is further illustrated in Fig. 7 by plotting deviations of the peak PL intensities divided by the average values (a) and the peak energies (b). For all compositions, the ratio of the intensity deviation and the average intensity is below 0.07, and for the low In content, it is as small as 0.03. The peak energy deviations are also small. For the In content up to 0.31, the peak energy deviation is only 6 to 8 meV; only for the In percentage around 35%, it increases up to 10 to 12 meV.

The spatial peak energy variations in the QWs may be determined by well width and alloy composition variations in the QW bulk and at the interfaces. The interfaces may influence SNOM results via spatially nonuniform cation interdiffusion and monolayer thick islands of different compositions, as observed in GaSb/AlGaSb QWs.[19] In order to determine the prevailing cause for the peak energy variations in our QWs, let us discuss these possibilities.

Band structure calculations show that monolayer fluctuations of the QW width would induce large PL peak energy shifts, from 24 meV for the 11% In QW to 54 meV for the 36% In QW. These variations are much larger than the peak energy variations observed in the SNOM scans. Thus, the well width fluctuations can hardly be considered as the main cause for the features of the peak wavelength maps.

Considering the influence of the spatial fluctuations of the well/barrier interfaces, one should note that the interface quality in $(20\bar{2}1)$ QWs is high. The interface abruptness and the atom distribution in $(20\bar{2}1)$ and $(20\bar{2}\bar{1})$ QWs with ~17% In were recently studied by the atom probe tomography.[20] For both planes, abrupt interfaces with the interface width of 0.2 nm were observed. No islands of different compositions were detected. Moreover, in Ref. 1, it was shown that the interface sharpness in $(20\bar{2}\bar{1})$ QWs is maintained over hundreds of nm. Assuming that the interfaces in the high In content QWs could be somewhat wider — say, 0.5 nm for both interfaces, the interface region would correspond to about 1/6 of the well width. To account for the peak energy variations observed in the SNOM scans, that would require about 6 times larger spatial variations of the alloy composition at the interfaces compared to that in the bulk of the QW. Considering the interface abruptness and its spatial uniformity mentioned above, this seems rather unlikely. Thus, most probably, it is the alloy composition variations in the bulk of the QW that give the main contribution of the spatial PL variations observed by the SNOM.

Assigning the peak energy variations solely due to the alloy composition fluctuations, the peak energy variations correspond to fluctuations of the InN molar fraction of only 0.03 for the QWs with In content up to 31% and 0.05 for those around 35%. Moreover, these numbers give the upper limit of the average alloy composition variations, since the interface properties may still have some effect on the peak energy distribution. Clearly, apart from eliminating the 100 nm scale PL variations, optimization of the growth conditions significantly increases the overall uniformity of alloy composition in the QWs.

Dependence of the average NF PL FWHM on the InN molar fraction is shown in Fig. 8. With the increase of the In content, the peak broadens from 100 to 170 meV. Interestingly, for higher excitation power densities, the linewidth was found to remain constant for the $In_{0.11}Ga_{0.89}N$ QW and slightly narrow for the higher In content QWs.[21]

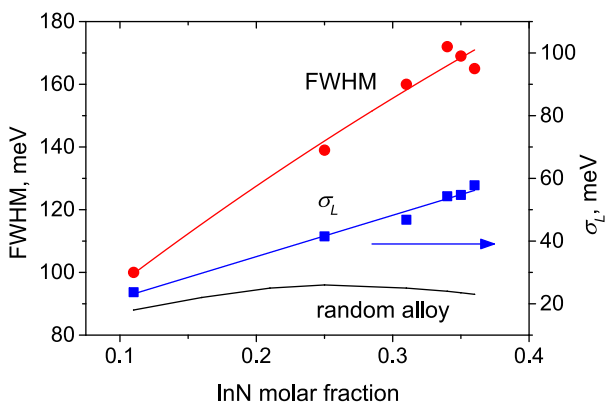

FIG. 8. Experimental values for the average FWHM and calculated values of the localization parameter σ_L and the linewidth for a random alloy. The lines are guides to the eye.

This effect was attributed to the enhanced carrier transfer towards the lower potential sites. No PL broadening due to state filling was observed.

In general, when discussing linewidths, one should note an essential difference between the PL linewidth measured in the far- and the near-field. In the far-field measurements, the linewidth includes band gap variations occurring within the measurement spot, which is typically tens of μm. In the near-field, the larger scale (>100 nm) band gap variations are revealed in peak wavelength maps shown above. Only the band potential variations occurring within the probe aperture influence the NF FWHM.

The FWHM values include homogeneous and inhomogeneous broadening contributions, $\Gamma = \Gamma_h + \Gamma_{ih}$. The homogeneous broadening is induced by carrier/exciton scattering by acoustic and LO phonons.[22,23] The temperature dependence of the homogeneous broadening is expressed as

$$\Gamma_h(T) = \beta T + \frac{\gamma}{\exp(\hbar\omega_{LO}/k_B T) - 1}.$$

Here β and γ define the exciton coupling strength with acoustic and LO phonons, respectively, and the second term is proportional to the Bose function of LO phonon occupation. Following the procedure used for GaN,[24] acoustic and LO phonon contributions to Γ_h can be evaluated from the temperature dependence of the PL linewidth. Fits of far-field PL measured at different temperatures for nonpolar[25] and $(20\bar{2}1)$ InGaN QWs for $0.11 \leq x \leq 0.20$ provide room temperature homogeneous broadening of 42 to 46 meV. One should note that the model used for Γ_h estimation assumes that Γ_{ih} does not change with temperature, which limits its applicability to materials with a weak localization, in which the temperature-activated carrier redistribution between higher and lower potential sites can be neglected. Therefore, estimation of Γ_h has been performed only for QWs with a small In content.

The estimated homogeneous linewidth can be compared to previous results. By using a deconvolution procedure of Γ_h and Γ_{ih} contributions to PL spectra of *c*-plane $In_{0.15}Ga_{0.85}N$ QW, Christmann *et al*. obtained room temperature homogeneous broadening of 29 meV.[25] For GaN, Γ_h values of 22 meV (Ref. 23) and 20 meV (Ref. 26) were reported. The larger homogeneous broadening in InGaN QWs compared to GaN can be explained by a larger number of phonon modes, including interface modes. One should note that, according to the calculations, the phonon energies and the exciton-phonon coupling in InGaN QWs are composition dependent;[27] thus, Γ_h should also depend on the alloy composition. However, these dependencies for the studied composition range $(0.11 \leq x \leq 0.36)$ are weak. Thus, composition dependence of Γ_h should be considerably smaller than that of Γ_{ih} and is not taken into account.

As discussed before, the inhomogeneous broadening is primarily induced by the band gap fluctuations due to the variation of the alloy composition. These fluctuations can be evaluated using a model, which — for the localized states — assumes a Gaussian distribution of the joint density of states[28]

$$g_G(E) = \int_{-\infty}^{+\infty} \frac{1}{\sqrt{2\pi}\sigma_L} \exp\left(-\frac{E_1^2}{2\sigma_L^2}\right) g_0(E - E_1) dE_1.$$

Here $g_0(E)$ is the density of states of an ideal QW with no localized states, and σ_L is the localization depth parameter, which describes the variation of the localized state band gap values. At room temperature and low excitation power densities, the carrier/exciton distribution obeys Boltzmann statistics; hence, the PL intensity is proportional to $I_{PL}(E) \propto g_G(E)\exp(-E/k_B T)$. Using the experimental data of the NF PL linewidths and the homogeneous broadening of 44 meV, the localization parameter for different studied QWs was found to be between 27 and 55 meV (Fig. 8, Table I).

The inhomogeneous broadening of the NF spectra may arise from the larger scale (tens of nm) band gap variations, or can be due to the random cation distribution. The difference between these mechanisms is that the first one could, probably, be reduced via development of the growth technology, while the second one could hardly be avoided. The influence of the random cation distribution on the inhomogeneous broadening has been theoretically investigated by Lee and Bajaj for excitons in AlGaAs at low temperature.[29] In 3 nm semipolar InGaN QWs, the exciton binding energy is about 40 meV,[30] considerably larger than the room temperature $k_B T$. Thus, it is reasonable to assume that at low and moderate carrier densities PL at room temperature is dominated by the exciton recombination. Recent studies on AlGaN and InGaN QWs support this assumption.[31,32] This allows applying the model of Lee and Bajaj to the NF spectra of our $(20\bar{2}1)$ InGaN QWs. According to the model, the FWHM induced by the perfectly random cation distribution σ_r is expressed as

$$\sigma_r = 2\frac{dE_g}{dx}\sqrt{\frac{2\ln 2x(1-x)\Delta V}{V_{ex}}}.$$

Here, ΔV is the volume of the unit cell, and V_{ex} is the exciton volume $V_{ex} = (4\pi/3)[\varepsilon\varepsilon_0\hbar^2/(\mu e^2)]^3$, where $\varepsilon = \varepsilon(x)$ is the static dielectric constant and μ is the reduced mass. As pointed out in Ref. 29, the exciton volume is not a well-defined quantity, which may lead to errors in estimation of the PL linewidth broadening caused by the random cation distribution. Even excluding the explicit usage of V_{ex}, the authors of Ref. 29 found that in high quality unstrained AlGaAs the calculated PL linewidths were 1.5 times smaller than the experimental data. Nevertheless, the model is meaningful for the relative comparison of samples with different alloy compositions.

The calculated FWHM for the random InGaN alloy of different compositions is plotted in Fig. 8. In the calculations, the composition dependent $In_xGa_{1-x}N$ band gap bowing parameter $b = 1.74 - 0.68x$ from Ref. 33 was used. The static dielectric constant and the effective mass values were taken from Ref. 34. The calculated random alloy broadening includes 44 meV of the homogenous broadening. As can be noticed, the linewidth shows little composition dependence

for $0.11 \leq x \leq 0.36$. According to the calculations, the strongest increase occurs at smaller x values.

Comparing the experimental and the calculated data, one can see that for $x = 0.11$, the values are close. With increased indium content, the experimental linewidths progressively exceed the ones for the random alloy. This shows that the sub-100 nm scale band potential variations increase with the InN molar fraction, which is consistent with the increase in the localization parameter σ_L. The large (μm) scale potential variations also increase with the In content, as evidenced by the larger peak energy deviations of the SNOM maps. Interestingly, recent NF measurements at different excitation powers have shown that lateral carrier transport between microscopic different potential sites in $(20\bar{2}1)$ QWs is limited.[21] This suggests that hot spot formation, caused by the lateral carrier transport into lower potential areas, in $(20\bar{2}1)$ QW photonic devices is unlikely, which should contribute to their longevity.

It is instructive to compare the measured linewidths with near-field PL data obtained for other $(20\bar{2}1)$ samples and InGaN QWs of other crystallographic orientations. In 30% In $(20\bar{2}1)$ QW, Kaneta *et al.* observed linewidths of 150–160 meV,[11] which is close to our results. However, in their study, the large-scale PL peak wavelength and intensity variations were much more pronounced. The peak wavelengths varied between 522 nm and 527 nm, and the relative integrated intensity — between 1 and 4 (the standard deviations were not reported). In $(20\bar{2}\bar{1})$ QWs with ~25% In, the smallest NF PL linewidths were 140–150 meV with peak energy deviations of 5–7 meV.[15] These values are similar to the ones reported in the current study. One should note, however, that the NF spectral parameters strongly depend on the sample quality: in a $(20\bar{2}\bar{1})$ QW sample grown under non-optimal conditions, the average FWHM and peak wavelength deviations were 197 meV and 28 meV, respectively.[15] Varying NF PL linewidths (150–240 meV for blue- and 160–180 meV for green-emitting QWs) and very strong variations of PL parameters were observed in a SNOM study of heteroepitaxial *c*-plane QWs.[7] A large PL intensity variation of up to 80 times was attributed spatial defect variations. In more recent confocal microscopy studies of green-emitting *c*-plane QWs, linewidths of ~120 meV (peak wavelength span between 536.9 nm and 539.5 nm, Ref. 35) and 200–300 meV (Ref. 9) were reported. Summarizing, one can notice that the NF PL linewidths in the semipolar and some of the polar QWs are quite similar, in spite that the large-scale band potential variations may strongly differ. This suggests that the NF PL linewidths, at least in narrow QWs with a moderate In content, have a common origin. It is tempting to assign this origin to the random cation distribution fluctuations. However, Fig. 7 shows that for QWs with all but the smallest InN molar fractions, the experimental linewidths considerably exceed those caused by the random cation distribution. Probably, both effects, the random cation distribution and the larger, 10-nm scale band potential variations contribute to the NF PL linewidths, with the latter contribution increasing with the In percentage.

Finally, let us look into the composition dependence of the correlation between the peak wavelength and the FWHM (Fig. 9). At low x values, there is no correlation between these parameters. The peak wavelength and the FWHM variations are miniscule, and the small-scale potential fluctuations, primarily determined by the random alloy broadening, are the same throughout the scanned area. For the intermediate In content (0.25 – 0.31), the correlation becomes positive, which means that spectra with longer peak wavelengths are broader. The positive correlation indicates that the exciton transfer from the higher to the lower potential sites is not efficient, because in the opposite case one would observe a spectral narrowing resulting in a negative r.

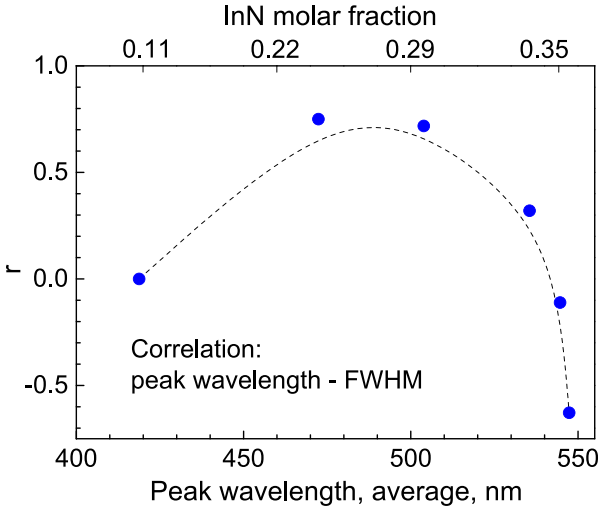

FIG. 9. Correlation between the peak wavelength and the FWHM for QWs with different In content. The line is a guide to the eye.

For the large InN molar fractions, the correlation coefficient decreases and, eventually, changes sign. In these QWs, the peak wavelength and the FWHM deviations as well as the FWHM average values are larger, indicating that the energy distribution of the localized states is wider and potential differences between the higher and the lower potential sites are more pronounced. The larger band gap variation might enhance the exciton transfer from the higher and the lower potential sites, resulting in narrower spectra for the longer peak wavelengths. One should, however, bear in mind that the peak wavelength and the FWHM variations, even in the highest In content QWs, are very small, and the provided interpretation applies only to a small fraction of excitons. This is an example how correlations between the NF PL maps, reflecting statistical data over thousands of spectra, amplify fine details that could not be detected by the standard far-field spectroscopy and allow a deeper insight into material properties.

V. SUMMARY

Scanning near-field optical spectroscopy has been applied to study spatial uniformity of emission spectra in semipolar $(20\bar{2}1)$ plane $In_xGa_{1-x}N/GaN$ ($0.11 \leq x \leq 0.36$) single QWs homoepitaxially grown on bulk GaN substrates. In general, the emission was found to be spatially uniform, with peak wavelength deviations in the range from 6 to 12 meV, and the ratios of the peak intensity deviations and the average values changing from 0.03 for the low In content

samples to 0.07 for $x \approx 0.35$. The maps of the near-field PL parameters showed large, a few μm size areas of similar values, contrary to 100 nm scale variations, often reported for InGaN QWs. These features confirm the high potential of $(20\bar{2}1)$ QWs for light emitting applications. The near-field spectra were found to broaden with the increased InN molar fraction. It is suggested that in the low In content QWs, the broadening is primarily determined by the random cation distribution, while for the larger InN molar fractions, 10 nm scale localization sites with increasingly deeper band potentials become important.

ACKNOWLEDGMENTS

M. Mensi and T. K. Uždavinys are acknowledged for AFM measurements. Research at KTH was performed within the frame of Linnaeus Excellence Center for Advanced Optics and Photonics (ADOPT) and was financially supported by the Swedish Energy Agency (Contract No. 36652-1) and Swedish Research Council (contract no. 621-2013-4096). Research at UCSB was supported by the Solid State Lighting and Energy Electronics Center (SSLEEC).

[1]D. F. Feezell, J. S. Speck, S. P. DenBaars, and S. Nakamura, J. Disp. Tech. **9**, 190 (2013).
[2]S. Yamamoto, Y. Zhao, C. C. Pan, R. B. Chung, K. Fujito, J. Sonoda, S. P. DenBaars, and S. Nakamura, Appl. Phys. Express **3**, 122102 (2010).
[3]M. Adachi, Y. Yoshizumi, Y. Enya, T. Kyono, T. Sumitomo, S. Tokuyama, S. Takagi, K. Sumiyoshi, N. Saga, T. Ikegami, M. Ueno, K. Katayama, and T. Nakamura, Appl. Phys. Express **3**, 121001 (2010).
[4]J. E. Northrup, Appl. Phys. Lett. **95**, 133107 (2009).
[5]A. Pinos, S. Marcinkevičius, J. Yang, Y. Bilenko, M. Shatalov, R. Gaska, and M. S. Shur, Appl. Phys. Lett. **95**, 181914 (2009).
[6]F. Hitzel, G. Klewer, S. Lahmann, U. Rossow, and A. Hangleiter, Phys. Rev. B **72**, 081309(R) (2005).
[7]A. Kaneta, M. Funato, and Y. Kawakami, Phys. Rev. B **78**, 125317 (2008).
[8]H. Itoh, S. Watanabe, M. Goto, N. Yamada, M. Misra, A. Y. Kim, and S. A. Stockman, Jpn. J. Appl. Phys., Part 2 **42**, L1244 (2003).
[9]D. Dobrovolskas, J. Mickevičius, E. Kuokštis, G. Tamulaitis, M. Shur, M. Shatalov, J. Yang, and R. Gaska, J. Phys. D: Appl. Phys. **44**, 135104 (2011).
[10]Y. Kawakami, K. Nishizuka, D. Yamada, A. Kaneta, M. Funato, Y. Narukawa, and T. Mukai, Appl. Phys. Lett. **90**, 261912 (2007).
[11]A. Kaneta, Y.-S. Kim, M. Funato, Y. Kawakami, Y. Enya, T. Kyono, M. Ueno, and T. Nakamura, Appl. Phys. Express **5**, 102104 (2012).
[12]A. Pinos, V. Liuolia, S. Marcinkevičius, J. Yang, R. Gaska, and M. S. Shur, J. Appl. Phys. **109**, 113516 (2011).
[13]H. Murotani, T. Saito, N. Kato, Y. Yamada, T. Taguchi, A. Ishibashi, Y. Kawaguchi, and T. Yokogawa, Appl. Phys. Lett. **91**, 231910 (2007).
[14]S. Marcinkevičius, K. M. Kelchner, S. Nakamura, S. P. DenBaars, and J. S. Speck, Appl. Phys. Lett. **102**, 101102 (2013).
[15]S. Marcinkevičius, Y. Zhao, K. M. Kelchner, S. Nakamura, S. P. DenBaars, and J. S. Speck, Appl. Phys. Lett. **103**, 131116 (2013).
[16]A. Pinos, S. Marcinkevičius, J. Yang, R. Gaska, M. Shatalov, and M. S. Shur, J. Appl. Phys. **108**, 093113 (2010).
[17]A. Pinos, S. Marcinkevičius, M. Usman, and A. Hallén, Appl. Phys. Lett. **95**, 112108 (2009) and references therein.
[18]F. Wu, Y. Zhao, A. Romanov, S. P. DenBaars, S. Nakamura, and J. S. Speck, Appl. Phys. Lett. **104**, 151901 (2014).
[19]X. Chen, Y. Song, L. Zhu, S. M. Wang, W. Lu, S. Guo, and J. Shao, J. Appl. Phys. **113**, 153505 (2013).
[20]R. Shivaraman, Y. Kawaguchi, S. Tanaka, S. P. DenBaars, S. Nakamura, and J. S. Speck, Appl. Phys. Lett. **102**, 251104 (2013).
[21]S. Marcinkevičius, K. Gelžinytė, Y. Zhao, S. P. DenBaars, S. Nakamura, and J. S. Speck, Appl. Phys. Lett. **105**, 111108 (2014).
[22]S. Rudin, T. S. Reinecke, and B. Segall, Phys. Rev. B. **42**, 11218 (1990).
[23]A. K. Viswanath, J. I. Lee, D. Kim, C. R. Lee, and J. Y. Leem, Phys. Rev. B **58**, 16333 (1998).
[24]V. Liuolia, A. Pinos, S. Marcinkevičius, Y. D. Lin, H. Ohta, S. P. DenBaars, and S. Nakamura, Appl. Phys. Lett. **97**, 151106 (2010).
[25]G. Christmann, R. Butté, E. Feltin, J.-F. Carlin, and N. Grandjean, Phys. Rev. B **73**, 153305 (2006).
[26]S. J. Xu, L. X. Zheng, S. H. Cheung, M. H. Xie, S. Y. Tong, and H. Yang, Appl. Phys. Lett. **81**, 4389 (2002).
[27]W.-D. Huang, G.-D. Chen, and Y.-J. Ren, J. Appl. Phys. **112**, 053704 (2012).
[28]P. G. Eliseev, P. Perlin, J. Lee, and M. Osinski, Appl. Phys. Lett. **71**, 569 (1997).
[29]S. M. Lee and K. K. Bajaj, J. Appl. Phys. **73**, 1788 (1993).
[30]S. Khatsevich and D. H. Rich, J. Phys.: Condens. Matter **20**, 215223 (2008).
[31]A. Pinos, S. Marcinkevičius, K. Liu, M. S. Shur, J. Yang, M. Shatalov, and R. Gaska, J. Phys. D: Appl. Phys. **41**, 155116 (2008).
[32]T. Langer, A. Chernikov, D. Kalincev, M. Gerhard, H. Bremers, U. Rossow, M. Koch, and A. Hangleiter, Appl. Phys. Lett. **103**, 202106 (2013).
[33]I. Gorczyca, T. Suski, N. E. Christensen, and A. Svane, Appl. Phys. Lett. **98**, 241905 (2011).
[34]S.-H. Park, D. Ahn, and S.-L. Chuang, IEEE J. Quantum Electron. **43**, 1175 (2007).
[35]M. Funato, Y. S. Kim, T. Hira, A. Kaneta, Y. Kawakami, T. Miyoshi, and S. Nagahama, Appl. Phys. Express **6**, 111002 (2013).